

Article

Increasing the Number of Material Recognition Classes in Cargo Inspection Using the X-Ray Dual High-Energy Method

Sergey Osipov ^{1,*} , Sergei Chakhlov ² and Eugeny Usachev ¹¹ Diagnostika-M LLC, Volgogradsky Av., 42, 109316 Moscow, Russia; usachev_e@x-ray.ru² Russian-Chinese Laboratory for Radiation Control and Inspection, School of Non-Destructive Testing, National Research Tomsk Polytechnic University, Lenina Av., 30, 634050 Tomsk, Russia; chakhlov@tpu.ru

* Correspondence: osip1809@rambler.ru

Abstract: Issues related to increasing the number of material recognition classes in cargo inspection by the X-ray dual high-energy method through introducing a class of heavy organic materials that include basic explosives are considered. A mathematical model of material recognition by the dual-energy method based on the parameters of level lines and effective atomic numbers has been proposed. Estimates of the parameters of the level lines and effective atomic numbers of explosives and their physical counterparts for monoenergetic and classical high-energy implementations of the dual-energy method were made. The use of a simulation model to demonstrate the ability to detect and correctly identify explosives and their physical counterparts using the dual high-energy method is illustrated. An algorithmic methodological approach is proposed to improve the accuracy of effective atomic number estimation. It has been demonstrated theoretically and by simulation that it is possible to distinguish materials in cargo inspection from the following classes of materials: light organics (typical representative—polyethylene); heavy organics (explosives), light minerals and heavy plastics (fluoropolymers); light metals (aluminum, $Z = 13$), heavy minerals (calcium oxide, $Z = 19$); metals (iron, $Z = 26$); heavy metals (tin, $Z = 50$); and radiation insensitive metals ($Z > 57$).

Keywords: cargo inspection; high-energy X-rays; dual-energy method; material recognition; explosives; effective atomic number; mass thickness; pre-filtering; ADC bit depth



Academic Editor: Andrés Amador Garcia-Granada

Received: 25 December 2024

Revised: 28 January 2025

Accepted: 30 January 2025

Published: 6 February 2025

Citation: Osipov, S.; Chakhlov, S.; Usachev, E. Increasing the Number of Material Recognition Classes in Cargo Inspection Using the X-Ray Dual High-Energy Method. *Computation* **2025**, *13*, 41. <https://doi.org/10.3390/computation13020041>

Copyright: © 2025 by the authors. Licensee MDPI, Basel, Switzerland. This article is an open access article distributed under the terms and conditions of the Creative Commons Attribution (CC BY) license (<https://creativecommons.org/licenses/by/4.0/>).

1. Introduction

High-energy inspection systems (HEISs) with the function of the detection of test object (TO) materials and their fragments by dual-energy methods (DEMs) are still one of the most effective and sort after technical means of customs control and X-ray cargo inspection [1–4]. The objective of the cited works is to discuss methods, approaches, and algorithms for recognition (distinction and classification) of materials using the dual-energy method. Multi-energy methods (MEMs) [3,5–9] are an evolution of DEMs and allow for an increase in the number of classes of recognized materials or the extension of the limits of applicability of DEMs for complicated structures of TOs. The unifying objective of the noted works is to illustrate the additional possibilities of material recognition using MEMs compared to DEMs. The recognition of the TO material or its structural fragment is understood as the unique belonging of the studied material to one of the given classes of materials based on a feature called recognition parameter (RP) [5]: “Limit capabilities of identifying materials by high dual- and multi-energy methods”. The main types of RPs associated with high-energy DEV and MEM realizations are estimates of the effective atomic number (EAN) of the TO material or the ratio of TO thicknesses in mean free paths

(MFPs) for low and high energies of bremsstrahlung (high-energy X-rays) [1,10–13]. The objective of the cited works is to analyze the features and compare the methods of material recognition using various dual-energy methods as applied to cargo inspection. In the scientific literature, the effective atomic number is usually denoted by the symbol Z_{eff} [2,4,13]. The physical process of detecting TO fragments and recognizing their materials by one of the recognition parameters is reduced to obtaining the initial digital radiographic DEM images, calibrating the obtained images “by black” and “by white”, taking the logarithm of the calibrated images, forming an image of the recognition parameter, correlating the value of the recognition parameter at each point of the image using special predetermined calibration functions (lines) to the recognition class, coloring all points of the image according to the selected palette in accordance with the calculated recognition class. The resulting final DEM image is analyzed by the operator or a specially developed algorithm in order to establish the correspondence or non-correspondence of the final TO image to the documentation accompanying the cargo. In the initial stage of the development of HEISs with the function of material recognition by DEMs, no more than four classes of materials were distinguished [14]—“Processing of interlaced images in 4–10 MeV dual-energy customs system for material recognition”—and these four classes were maintained until recently [15]: “A curve-based material recognition method in MeV dual-energy X-ray imaging system”. A typical representative of the first class was polyethylene, the second was aluminum or its alloys, the third, iron or its alloys, and the fourth, lead. All major HEIS manufacturers guarantee correct material identification for three to four classes [16–21]. The objective of this work is to demonstrate modern trends towards expanding the number of classes of materials recognizable by the low-energy dual-energy method. In the above-mentioned HEIS, betatrons or linear accelerators are used as sources of high-energy X-ray radiation. The objects under control are scanned by narrow beams of high-energy X-ray (bremsstrahlung) radiation with alternating maximum energies from pulse to pulse (from one group of pulses to another). High energy is determined by the maximum possible energy for the radiation source used; it is usually equal to 6 MeV, 7.5 MeV, or 9 MeV. Low energy is usually 2–3 MeV less than high energy. The website [21] refers to the possible correct identification of four or more classes of materials. In the range of maximum energies of X-rays from 50 to 250 keV, where two effects of the interaction of gamma rays with matter compete—the photoelectric effect and the Compton effect—the number of classes of correctly recognized materials has expanded considerably in recent years [22–24]. Work [5] highlights that the increase in the number of classes of materials that can be detected during a high-energy inspection is associated with physical limitations due to the interaction of high-energy (energy above 1.022 MeV) gamma rays with matter. It is known that, at energies from 2 to 10 MeV, the Compton effect and the electron–positron pairs effect compete [25]—“Photon cross sections, attenuation coefficients and energy absorption coefficients”—and the mass attenuation coefficient (MAC) of photons corresponding to the pair birth effect is proportional to EAN [26], “Electron-positron pair production by photons: A historical overview”, and for small values of EAN, the contribution of pairs to the integral MAC is insignificant. The insignificance of the change in the integral MAC in the range of small values of EAN is the main obstacle to increasing the number of classes of correctly recognized materials [27]: “Automated X-ray image analysis for cargo security: Critical review and future promise”. In [27], questions concerning the high-energy realization of DEMs are formulated. The need for a comparative study of different image preprocessing methods [27] is certainly related to increasing the number of classes of correctly recognized materials. Moreover, [27] raises the following question: Will machine learning-based material recognition perform better than current implementations of DEMs based on the physics of the interaction between bremsstrahlung and matter? In [27], the strong noise in the initial

and final images of DEMs in commercial HEISs is pointed out, which partially limits the ability to increase the number of recognition classes. The work [27] illustrates the complexity of correct material recognition of objects (fragments) with small and large thicknesses. The incorrect recognition is due to a pronounced difference in the energy spectrum of the bremsstrahlung of the delta function (monoenergetic gamma-ray source) on the one hand and a high level of noise in the original digital radiographic images and (or) a low level of digital signals on the other hand. Quantum or pseudo-quantum starvation leads to a low level of digital signals [28], “Increasing penetrating power of digital radiography systems based on analysis of low-intensity signals”. Quantum starvation is caused by insufficient photons registered by detectors behind a large TO [28], and pseudo-quantum starvation by insufficient ADC bit depth [28,29]. In order to improve the quality of recognition of small material thicknesses, it is quite effective to convert the sources of bremsstrahlung radiation into pseudo-monoenergetic ones by introducing pre-filtering of photons [29]—“Physical and technical restrictions of materials recognition by the dual high energy X-ray imaging”—which, however, leads to the amplification of the effect of quantum and/or pseudo-quantum starvation. Work [14] states that the main direction of the development of HEISs with the function of material recognition by the dual and multi-energy method in the last two decades is mainly associated with an increase in the productivity and quality of material recognition. The work [30], “Security in the maritime container supply chain: what is feasible and realistic?”, emphasizes that the growth of international trade, especially through container shipping, is accompanied by the emergence of various types of smuggling, including drugs, weapons, cigarettes, explosives, radioactive and nuclear substances, and the potential risks and threats associated with these activities are also increasing. The work [30] states that in order to meet the corresponding challenges and threats, customs authorities, border guards, and transport security units must significantly strengthen the monitoring of transported goods and vehicles by improving the technical means of high-energy X-ray inspection and ensuring their necessary number for the benefit of consumers and the prevention of the illegal transport of particularly dangerous goods. The work [5] assumes an increase to five classes of materials correctly recognized by high-energy dual and multi-energy methods and also theoretically and experimentally demonstrates the fundamental possibility of distinguishing the following classes of materials: light organics ($Z_{eff} = 6$); minerals ($Z_{eff} = 9$); light metals ($Z_{eff} = 13$); calcium ($Z_{eff} = 19$); metals ($Z_{eff} = 26$); and heavy metals ($Z_{eff} > 50$). It was noted above that for high-energy DEM implementations, the competing processes of interaction of gamma radiation with matter are the Compton effect and the pair birth effect, therefore, with an increase in EAN; therefore, the features of recognition of materials with high EAN values are determined by the MAC dependencies for the Compton effects and pair production on EAN [4,5,11,14]. An article [12], “Material Estimation Method Using Dual-Energy X-Ray Image for Cargo Inspection System”, compares the quality of the material recognition algorithms of DEMs with the increased number of classes of correct recognition. Theoretically, it justifies the possibility of distinguishing classes of materials associated with acrylic ($(C_5O_2H_8)_n$), carbon (C), water (H_2O), aluminum (Al), iron (Fe), tin (Sn), and lead (Pb). It should be noted that, in the results of the experiments [12], data on the test samples with water are missing, which most likely indicates insufficiently correct recognition of this material.

The problem of increasing the recognition classes of TO materials and their structural fragments by DEMs is still relevant, especially in the range of EAN values from 5 to 13, due to the need to detecting and correctly recognize explosives and drugs [2]: “Raw data processing techniques for material classification of objects in dual energy X-ray baggage inspection systems”. In a recent work [31], “Dose Evaluation of a Car Occupant in Dual Energy X-Ray Automobile Inspection System”, it is pointed out that it is necessary to

diagnose the nature of the substance in the case of drugs with low atomic number, as well as in the case of many explosives, such as plastic explosives, which can be masked in various ways. The article [32], “Development of a Dual-Modality Gamma-ray/Fast Neutron Imaging System for Air Cargo Inspection”, argues that cargo inspection systems using high-energy bremsstrahlung sources (the equivalent term, according to the authors of [32], is gamma-ray, which is controversial) are limited in detecting objects of low-density materials, such as drugs or plastic explosives. Therefore, the combined use of bremsstrahlung and neutron sources is proposed, which will allow a strong expansion of the detection of the mentioned materials. In the conclusion of the work [32] on the achievement of bremsstrahlung (high-energy X-rays) HEISs, its limit in terms of material recognition seems not sufficiently argued. So, theoretical, simulation, and experimental studies on the evaluation and achievement of DEM limits in terms of correct material recognition in cargo inspection in the range of small values of EAN are needed.

2. Materials and Methods

The introduction points out the purpose of the research—to evaluate the possibility of increasing the number of material recognition classes by dual high-energy methods, preferably for low values of EAN.

2.1. Materials

It has already been mentioned that the greatest threats and risks are associated with the illegal movement of explosives, drugs, and weapons.

Table 1 shows the chemical formulas and estimated experimental values from EAN for some organic and inorganic materials, metals, and explosives. The materials traditionally used for calibration in DEM are marked in bold. The difference in the values of effective atomic numbers is due to various methods for estimating EAN [33–35]. This fact is unacceptable since any measurement (estimates) must have the property of reproducibility; this is also true for various applications of DEM [36–38].

Table 1. Chemical formulas and effective atomic numbers of materials.

Material and Chemical Substance	Chemical Formula	Theoretical Estimates Z_{eff}	Experimental Values Z_{eff}
Polyethylene	$(CH_2)_n$	5.4	
Carbon (graphite)	C	6	6
Sugar	$C_{12}H_{22}O_{11}$	6.92 [23]	
Water	H_2O	7.49 [34]	
Trinitrotoluene	$C_7H_5N_3O_6$	7.27 [34], 7.09 [35]	
RDX	$C_6H_6O_6N_6$	7.41 [34], 7.11 [35]	
C-4	$C_3H_6O_6N_6$	7.34 [33], 7.26 [35]	
Pentrite	$C_5H_8O_{12}N_4$	7.58 [33], 7.43 [35]	
Borax	$Na_2B_4O_7 \cdot 10H_2O$	8.06 [23]	
Fluoropolymer	$(C_2F_4)_n$	10.0 [36], 8.5 [37]	
Albite	$NaAlSi_3O_8$	11.62 [33], 11.44 [35]	11.22 [33]
Quartz	SiO_2	11.85 [33], 11.24 [34], 11.67 [35]	
Aluminum	Al	13	13
Dolomite	$CaMg(CO_3)_2$	13.94 [33], 13.33 [35]	13.61 [33]
Calcite	$CaCO_3$	15.88 [33], 15.26 [35]	
Fluorite	CaF_2	16.98 [33], 16.76 [35]	
Rutile	TiO_2	19.3 [33], 18.6 [35]	19.4 [33]
Pyrite	FeS_2	22.21 [33], 21.59 [35]	
Iron	Fe	26	26
Tin	Sn	50	50
Lead	Pb	82	82

2.2. Classification of Materials by the Dual-Energy Method

The introduction emphasized that the totality of materials transported by vehicles is divided into several detection groups by the dual-energy method. The classification of materials into groups closest to the subject of this article can be found in [23] (see Table 2). This classification is given for low-energy implementations of the DEM, and the names of the classes are rather conditional.

The work [5] classifies materials close to [23], where each recognition class is associated with the EAN of its typical representative, i.e., the vector \mathbf{Z}_{eff} defines the set of recognition classes. For example, the vector $\mathbf{Z}_{eff} = \{6, 9, 13, 19, 26, 50, 65\}$ was analyzed in [5].

Table 2. Classification of materials by the dual-energy method [23].

\mathbf{Z}_{eff}	Class of Materials
1–8	Organic materials
8–10	Light inorganic materials
10–12	Heavy inorganic materials
12–17	Light metals
17–29	Heavy metals
29+	Superdense metals
–	Non-transparent materials

From the above and the purpose of this work, it follows that it is necessary to divide the class of organic materials into two classes—light and heavy organic materials. From Table 1, we can conclude that it is logical to assign polyethylene to the class of light organic materials. According to Table 1, water can be associated with the class of heavy organic materials, which includes the main explosives. Sugar (the lower limit of the class of heavy organic materials according to EAN) and borax (the upper limit of the class of heavy organic materials according to EAN) can also be used for imitation explosives. It should be noted that using water as a calibration material for DEMs is difficult. For low-energy DEM realizations, non-explosive explosion simulators [39] that correspond to actual samples in density and elemental composition are used. However, creating such simulators for high-energy DEM implementations is quite difficult, since it is a liquid in the temperature range from 1 to 100 degrees Celsius. An alternative could be the approach proposed in [35], based on B-Al equivalents of explosives by effective atomic number.

3. Mathematical Model of Material Recognition by the Dual High-Energy Method

3.1. Mathematical Model of Material Recognition by Dual-Energy Method by Level Lines

One of the most effective implementations of DEMs and MEMs is the method of level lines [1,5,12,14,15,29]. In the case of DEMs, the identification parameter is the ratio of the estimates of Q for the TO thicknesses in the MFP y_H for the higher maximum bremsstrahlung energy E_H to y_L for the lower maximum bremsstrahlung energy E_L . Here, and below, the index L relates the indexed value to the low maximum energy of bremsstrahlung E_L (low-energy), and the index H corresponds to the high maximum energy of bremsstrahlung E_H (high-energy).

The mathematical model of material recognition by the dual high-energy method consists of the following blocks:

- Mathematical model of material recognition by Dual-Energy Method by Level Lines
 - Mathematical Model for Estimating the TO Thickness in Free Run Lengths
 - Material Recognition Criteria by Level Line Method

- Recognition Parameter in the DEM Implementation by the Level Lines Method
- Recognition Calibration in the DEM Implementation by the Level Lines Method
- Material Recognition Criteria by Level Line Method
- Estimation of the Effective Atomic Number by the Dual High-Energy Method
 - Monoenergetic Implementations of DEMs
 - Non-monoenergetic DEM Implementation.

Mathematical models of the formation of primary radiographic images [5,8,29], taking into account the modification [28], were chosen as the basis for calculating the dependence of the estimates y_L and y_H on the parameters of the HEIS and TO. All the models mentioned are based on the Bouguer–Lambert–Beer attenuation law, valid for monoenergetic gamma ray in parallel beam geometry, and generalized to the case of an X-ray source with a continuous spectrum and photon registration by an integrating detector that is not a total absorption detector. The models mentioned are based on tabulated dependences of the mass attenuation coefficients of gamma rays on the energy and atomic number of the attenuating substance [25,26].

3.1.1. Mathematical Model for Estimating the TO Thickness in Free Run Lengths

The dual-energy recognition HEISs are high-energy digital radiography systems that are characterized by a number of basic parameters related to the source and detector of bremsstrahlung radiation, as well as to the test object.

Parameters of the bremsstrahlung radiation source:

- maximum energies of the bremsstrahlung E_L, E_H , MeV ($E_L < E_H$);
- numerical energy spectra of the bremsstrahlung source for maximum energies E_L and $E_H - f(E, E_L), f(E, E_H)$;
- pulse repetition rate ν , Hz;
- the average number of photons emitted by the source in one pulse (subscript “1”) and falling on the front surface of the radiation-sensitive element (RSE) of the detector, for maximum energies E_L and $E_H - N_{1L}, N_{1H}$;
- number of bremsstrahlung pulses for generating digital signals for maximum energies E_L and $E_H - n_L, n_H$;
- density, material atomic number, and pre-filter thickness— ρ_f, Z_f, h_f .

Proton prefiltering leads to a transformation of the numerical energy spectra of bremsstrahlung $f(E, E_L), f(E, E_H)$ in $f_L^*(E), f_H^*(E)$

$$f_L^*(E) = f(E, E_L) \exp\left(-m(E, Z_f)d_f\right), f_H^*(E) = f(E, E_H) \exp\left(-m(E, Z_f)d_f\right), \quad (1)$$

where $m(E, Z_f)$ is the mass attenuation coefficient (MAC) of gamma radiation with energy E by a material with atomic number Z_f . The superscript “*” in (1) denotes the transformation of the numerical energy spectrum.

Bremsstrahlung detector parameters:

- chemical formula of the RSE detector substance *Chemd*

$$Chemd = \bigcup_{i=1}^{n_d} (A_{di}, p_{di}), \quad (2)$$

where n_d is the number of chemical elements that form the RSE substance; A_{di}, p_{di} are a designation of the i -th chemical element and the number of its atoms in the molecule. Here and below, the subscript “d” is associated with the detector (RSE);

- RSE detector thickness and density of its material h_d , cm, ρ_d , g/cm³;
- ADC bit depth k_{ADC} , bits;
- degree of filling of the digital signal range C_{ADC} ;
- maximum TO thickness in mean free paths $P(E_{\max})$, MFP;
- minimum digital signal level M .

The vector $\mathbf{A}_d = (A_{d1}, A_{d2}, \dots, A_{dn_d})$ uniquely determines the vectors of molar masses and atomic numbers of elements $\mathbf{M}_d = (M_{d1}, M_{d2}, \dots, M_{dn_d})$, $\mathbf{Z}_d = (Z_{d1}, Z_{d2}, \dots, Z_{dn_d})$ [40].

The above is also true for any chemical substances, i.e., for any vector \mathbf{A} , it is true $\mathbf{A} \Leftrightarrow (\mathbf{M}, \mathbf{Z})$. Vectors \mathbf{M} , \mathbf{Z} and \mathbf{p} allow us to calculate the MAC $m(E)$ for any chemical substance and photons with energy E

$$m(E, \mathbf{A}, \mathbf{p}) = \sum_{i=1}^{nc} p_i M_i m(E, Z_i) / \sum_{i=1}^{nc} p_i M_i, \quad (3)$$

where nc is the number of elements in the vectors \mathbf{M} , \mathbf{Z} , and \mathbf{p} .

The bremsstrahlung detector characterizes most completely the dependence of the detection efficiency on the energy

$$\varepsilon_d(E) = 1 - \exp(-m(E, \mathbf{A}_d, \mathbf{p}_d) \rho_d h_d). \quad (4)$$

To describe TO, we introduce a fixed orthogonal coordinate system OXYZ. The origin of the coordinate system O is connected to the center of the radiating surface of the bremsstrahlung source. Let the inspection object be scanned by a narrow beam of bremsstrahlung, which is registered by a linear detector. Let us connect the axis OZ with the scanning direction and the axis OX with the detector line.

Test object parameters:

- the set of points \mathbf{V} of the three-dimensional space occupied by the TO, $\mathbf{V} \subset \mathbb{R}^3$;
- distribution of vectors \mathbf{A} , \mathbf{p} , and the density ρ of the material over the volume \mathbf{V} .

The degree of attenuation of radiation with energy E is completely determined by TO thickness in the MFP $P(E, x, z)$ along the ray $L(x, z)$ connecting the emitting point and the detection point with coordinates (x, z) . The formula for estimating $P(E, x, z)$ is

$$P(E, x, z) = \int_{L(x, z)} m(E, \mathbf{A}(x, y, z), \mathbf{p}(x, y, z)) \rho(x, y, z) dy. \quad (5)$$

Recall that for any point $(x, y, z) \in \mathbf{V}$ the vector $\mathbf{A}(x, y, z)$ is equivalent to a pair of vectors $(\mathbf{Z}(x, y, z), \mathbf{M}(x, y, z))$; that is, the MAC value in expression (5) is calculated using Formula (3).

Formula for estimating the analog signal from the detector

Taking into account the above notations and expressions, the formula for estimating the analog signal (AS) from the detector looks like

$$J(E_{L,H}, x, z) = C_E N_{1,L,H} \int_0^{E_{L,H}} E_{ab}(E) f_{L,H}^*(E) \exp(-P(E, x, z)) \varepsilon_d(E) dE + B(x). \quad (6)$$

Here, C_E is the coefficient of conversion of the absorbed bremsstrahlung energy into electric current energy; $B(x)$ is the energy equivalent of the dark current of the detecting element at the point with coordinate x ; $E_{ab}(E)$ is the average value of the registered photon energy.

Strictly speaking, $E_{ab}(E)$ depends on the sizes of the material and RSE, but for the problem in question, we can take $E_{ab}(E) \approx E$.

There are three types of AS from the detector element: the “dark” signal, i.e., the signal with the bremsstrahlung source turned off; the signal without attenuation, in this case, the bremsstrahlung radiation is on and $\int_{L(x,z)} \rho(x,y,z)dy = 0$; the measuring signal—the bremsstrahlung radiation is on and $\int_{L(x,z)} \rho(x,y,z)dy \neq 0$.

Converting analog signals to digital signals

Regardless of the type of AS, the formula $J_{L,H}(x,z)$ for describing the transformation into digital signals (DS) $D_{L,H}(x,z)$ has the following form

$$D_{L,H}(x,z) = \left\lfloor \frac{J_{L,H}(x,z)}{\Delta} \right\rfloor, \Delta = \frac{C_{ADC} J_{\max}}{2^{k_{ADC}} - 1}. \quad (7)$$

Here, J_{\max} is the maximum expected level of analog signals without attenuation $J_{\max} = \max_{(x,z) \in S_W} (J_L(x,z), J_H(x,z))$; S_W is the area of a preliminary evaluation of signals without attenuation from the detector elements. Here, the subscript “W” corresponds to calibration in white.

Calibration of digital signals and evaluation of TO thickness in mean free paths

Calibration of digital signals is reduced to the subtraction of average levels of digital “dark (black)” signals (subscript B) $D_{L,HB}(x)$, followed by normalization to the average levels of the calibrated “black” signals without attenuation $D_{L,HW}(x) - D_{L,HB}(x)$. The obtained values are converted into the corresponding estimates of TO thicknesses in MFP y_L, y_H . The final formula for estimation $y_{L,H}(x,z)$ is as follows

$$y_{L,H}(x,z) = -\ln \frac{\max(D_{L,H}(x,z) - D_{B,L,H}(x,z), 1)}{D_{W,L,H}(x,z) - D_{B,L,H}(x,z)}. \quad (8)$$

Let S be the projection of V on the XOZ plane, then the sets $Y_L = \{y_L(x,z) | (x,z) \in S\}$ and $Y_H = \{y_H(x,z) | (x,z) \in S\}$ the digital radiographic images of TO in the DEM. These images are fed to the input of the material identification block.

3.1.2. Material Recognition Criteria by Level Lines Method

Recognition Parameter in the DEM Implementation by the Level Lines Method

The recognition parameter in the considered DEM implementation is the ratio Q of the TO thickness in the EAN y_H for a higher maximum bremsstrahlung energy E_H to the TO thickness in the MFP y_L for a lower maximum bremsstrahlung energy E_L

$$Q(x,z) = \frac{y_H(x,z)}{y_L(x,z)}. \quad (9)$$

Recognition Calibration in the DEM Implementation by the Level Lines Method

Recognition calibration in the DEM implementation by the level lines method is necessary to correctly assign the TO material or its structural fragment to one or another class of recognizable materials.

Let there be n_Q classes of material recognition by the dual-energy method. Each j -th recognition class is associated with some material with an effective atomic number Z_{eff}^j . However, in accordance with (3), the chemical formula of the substance $Chem$ can be associated with the main material of the class.

Recognition calibration is reduced to determining the level lines $Qc_j(y_L)$, $j = 1 \dots n_Q$. For this purpose, an image of TO consisting of fragments whose effective atomic number of materials and their mass thicknesses overlap the zones of consumer interest is formed.

Here, the mass thickness of the TO (fragment) is understood as the product of its material density by the thickness. The table of functions $Qc_j(y_L)$ is the result of processing the images of the corresponding fragments of the test object for each line of level j . Approximations of functions $Qc_j(y_L)$ by polynomials with powers from 2 to 4 are introduced to simplify the algorithm of assigning the material of the studied fragment to the class with the corresponding level line.

Material Recognition Criteria by Level Line Method

The criterion of material recognition by the level lines method means some rule of attributing the current value of the pair $(y_L(x, z), Q(x, z))$ to one or another level line.

It seems most logical to refer the pair $(y_L(x, z), Q(x, z))$ to the nearest level line. In this case, the corresponding rule is formulated as follows: material at a point with coordinates (x, y) , values $y_L(x, z)$, and $Q(x, z)$ belongs to the j_0 -th class if

$$|Q(x, z) - Qc_{j_0}(y_L(x, y))| = \min_{j, j=1 \dots n_Q} |Q(x, y) - Qc_j(y_L(x, y))|. \quad (10)$$

The number of recognition classes is limited, so checking (10) is not time-consuming.

If necessary, the material recognition model based on the level lines method is supplemented by noise in the initial radiographic images, described, for example, in [8].

3.2. Estimation of the Effective Atomic Number by the Dual High-Energy Method

The most important recognition parameter is the effective atomic number of the material Z_{eff} of the test object. This parameter is estimated using the same initial data y_L and y_H as in the level lines method.

There are two approaches to estimating EAN using the dual (multi-energy) method [13,29,35,41–45]. The first one is based on the MAC representation of gamma rays by the sum of MAC of two competing processes (the photoelectric effect with the Compton effect in the low-energy range of gamma rays and the Compton effect with the effect of pair production in the high-energy range of gamma rays) (Alvarez–Makovsky method). The second approach is based on a simultaneous evaluation of the EAN and the mass thicknesses. The second approach implicitly considers all the properties of the interactions of photons with matter and does not require precise information about the shape of the energy spectrum, the energy dependences of the MAC for the photoelectric effect, the Compton effect, and the effect of pair-birth production. If there are rationally formed test objects consisting of fragments of different mass thicknesses of materials with different EAN values, the second approach allows estimating mass thicknesses and effective numbers of TO materials with high accuracy.

Let us dwell on the monoenergetic implementation of DEM. The inclusion of this subsection pursues two specific goals: the first is to find an effective (highly accurate and high-performance) algorithm for estimating the effective atomic number of a material using the levels lines method; the second is to evaluate the ultimate capabilities of DEM based on high-energy monoenergetic gamma ray sources in relation to estimating the effective atomic number of a material. The ultimate capabilities of DEMs include the accuracy of Z_{eff} estimation and the range of Z_{eff} variation for which the effective atomic number is estimated with high accuracy.

3.2.1. Monoenergetic Implementations of DEMs

The specificity of monoenergetic DEM realizations consists of the proximity of the PR Q to the MAC for energies E_H and E_L

$$Q(x, z) = \frac{y_H(x, z)}{y_L(x, z)} \approx \frac{m_H(x, z)}{m_L(x, z)}. \quad (11)$$

From the analysis of (11), it follows the independence of Q from the mass thickness of the TO and the dependence on the EAN of the TO material Z_{eff}

$$Q(Z_{eff}(x, z)) = \frac{y_H(x, z)}{y_L(x, z)} \approx \frac{m_H(Z_{eff}(x, z))}{m_L(Z_{eff}(x, z))}. \quad (12)$$

If the discrete function $Q(Z)$ is monotone on Z in the range of interest of the consumer, for example, from 3 to 82, then the continuous monotone function $Q^*(Z)$, interpolating (approximating) $Q(Z)$, has the inverse function Q^{*-1} .

The formula for estimating Z_{eff} is

$$Z_{eff}(x, z) = Q^{*-1}\left(\frac{y_H(x, z)}{y_L(x, z)}\right). \quad (13)$$

To verify the monotonicity of the discrete function $Q(Z)$, the values of Q in the range Z from 3 to 82 were calculated. The results of the calculations are shown in Figure 1. Analyzing the results of the function $Q(Z)$ calculations, we see that the studied function is monotonic on the interval $3 \leq Z \leq 75$.

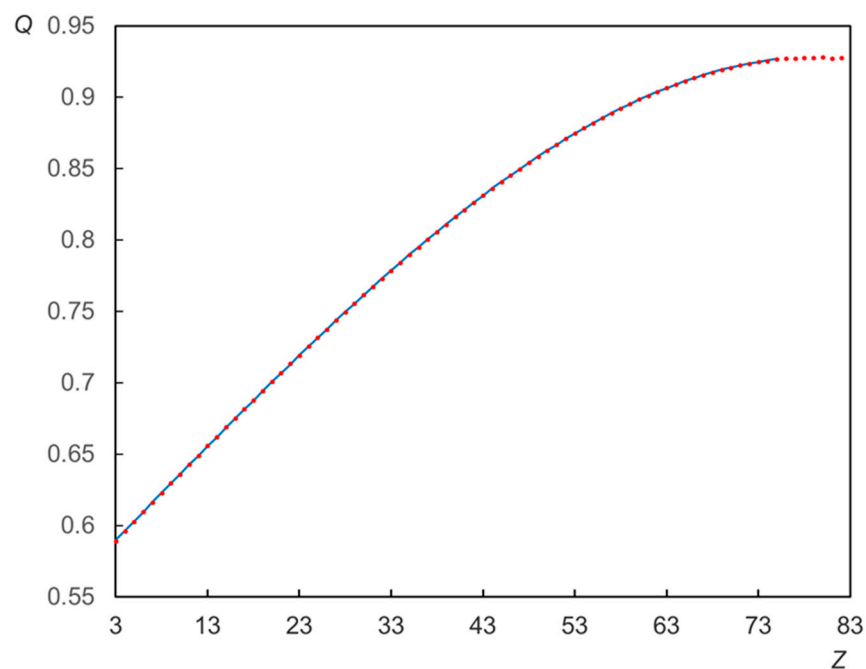


Figure 1. Dependence $Q(Z)$ for the monoenergetic DEM realization ($E_L = 2$ MeV, $E_H = 5$ MeV): ●—calculation; —approximation (14).

The derivative of the discrete function $Q(Z)$ is positive on the interval $3 \leq Z \leq 75$ and decreases to zero as Z increases. The function $-\ln(Q(Z))$ was approximated by a third-degree polynomial. The general form of the function $Q^*(Z)$, which approximates $Q(Z)$, has the form

$$Q^*(Z) = \exp(-AZ^3 - BZ^2 - CZ - D). \quad (14)$$

The approximation parameters $A = 1.00963 \times 10^{-7}$, $B = 0.00006$, $C = -0.01152$, and $D = 0.56175$ were found by the least squares method (14) for $E_L = 2$ MeV, $E_H = 5$ MeV.

Figure 1 shows the approximation of $Q(Z)$ by the function $Q^*(Z)$ (14).

The data presented in Figure 1 indicate that starting from a certain value of Z , the function $Q(Z)$ becomes flat. This factor leads to an increase in the error in estimating the atomic number Z based on the experimentally measured value of Q and to insufficient quality of recognition of materials with Z exceeding a certain level, for example, $Z = 56$.

Figure 2 illustrates the quality of estimating the effective atomic number Z_{eff} using Formulas (13) and (14).

From the analysis of the data of Figure 2, we can conclude about the hypothetical possibility of estimation of EAN by the high mono-energy dual-energy method in the range of Z_{eff} changes from 3 to 73 with an absolute error not greater than 0.35, and for the interval $3 \leq Z \leq 68$ the error will not exceed 0.1.

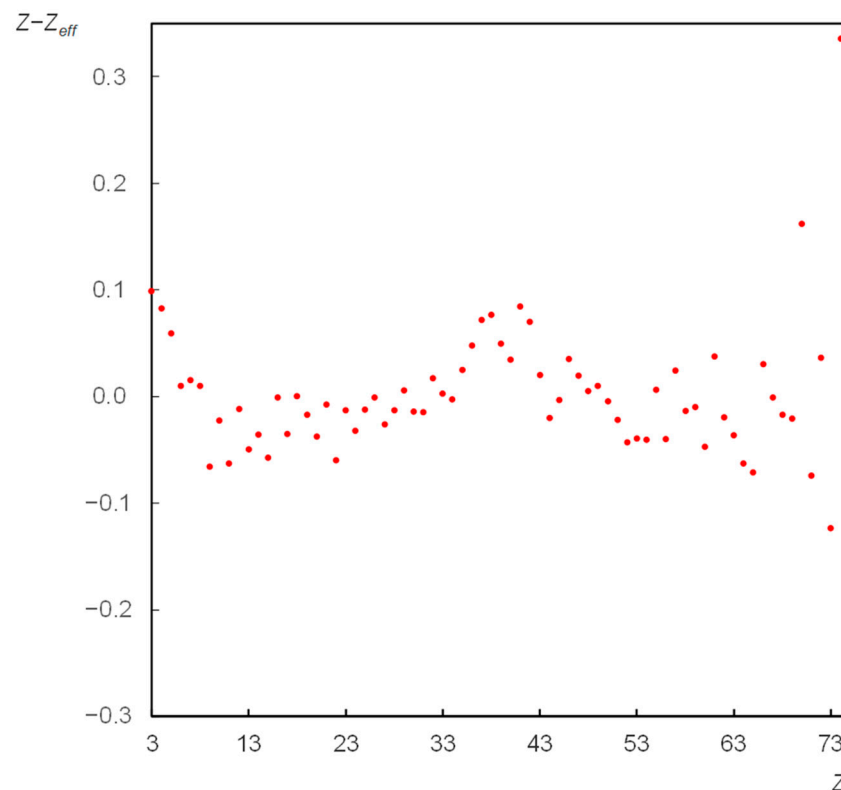


Figure 2. The dependence of the absolute estimate Z_{eff} for the monoenergetic DEM realization ($E_L = 2$ MeV, $E_H = 5$ MeV): • – dependence $Z - Z_{eff}(Z)$.

3.2.2. Non-Monoenergetic DEM Implementation

A specific feature of the use of non-monoenergetic DEM implementations for estimating EAH is the hardening of the bremsstrahlung spectrum with an increase in the mass thickness of the TO at a fixed value of the EAH or an increase in the EAH at a fixed mass thickness of the TO.

It is possible to simultaneously estimate the mass thickness of the TO and EAN of its material. For this, the system of two nonlinear equations is solved

$$\begin{cases} F_L((\rho H)_{eff}, Z_{eff}) = y_L(x, z) \\ F_H((\rho H)_{eff}, Z_{eff}) = y_H(x, z) \end{cases} \quad (15)$$

where $F_L((\rho H)_{eff}, Z_{eff})$, $F_H((\rho H)_{eff}, Z_{eff})$ are the DEM calibration functions for the maximum energies of the bremsstrahlung E_L and E_H .

From the analysis of the results shown in Table 3, we can conclude that the recognition of materials with low mass thicknesses is slightly incorrect for materials with an EAN value of 56 or more, despite the use of a 30 mm thick iron filter. Obviously, this is related to the range of monotonicity of the function $Q(Z)$. The mentioned moment is veiled and manifests itself directly when solving the system (16). Due to the importance of this point, we will consider it in detail in the Discussion section.

Overall, the noted conclusion corresponds to the results of [5,6].

4. Results

The materials from Table 1 were selected to evaluate the possibility of increasing the classes of material recognition by the high-energy DEM based on the level lines method. The studies were conducted by modeling based on the above mathematical models for a hypothetical monoenergetic DEM implementation and a realistic DEM implementation based on high-energy bremsstrahlung sources.

4.1. A Hypothetical Monoenergetic Realization of the Dual-Energy Method

It was noted in [5] that the conditions for the formation of initial images in the dual-energy methods are ideal if the following assumptions are met:

- energy spectra of radiation $f(E, E_L), f(E, E_H)$ are described by δ -functions;
- the detectors are total absorption detectors, i.e., $\epsilon(E_{L,H}) \approx 1$ and $E_{ab}(E_{L,H}) = E$;
- the number of photons incident on the detector surface for the maximum energies E_L and E_H is large; i.e., $N_{1L} \rightarrow \infty$ and $N_{1H} \rightarrow \infty$;
- the ADC bit depth is high, i.e., $k_{ADC} \rightarrow \infty$.

In most cases, the hypothetical monoenergetic DEM realization does not imply the existence of real gamma-ray energy lines. The necessity for modeling the hypothetical sources of gamma radiation is determined by eliminating the beam hardening effect, which is typical for high-energy DEM implementations when using bremsstrahlung sources.

Obviously, Formula (9) for the above idealized conditions will look like

$$Q(x, z) = \frac{\int_{L(x,z)} m(E_H, \mathbf{A}(x, y, z), \mathbf{p}(x, y, z)) \rho(x, y, z) dy}{\int_{L(x,z)} m(E_L, \mathbf{A}(x, y, z), \mathbf{p}(x, y, z)) \rho(x, y, z) dy}. \quad (18)$$

Recall that the material of the TO fragments is recognized correctly in the case of their spatial separation. In this case, expression (18) is transformed as follows

$$Q(x, z) = m(E_H, \mathbf{A}(x, y, z), \mathbf{p}(x, y, z)) / m(E_L, \mathbf{A}(x, y, z), \mathbf{p}(x, y, z)). \quad (19)$$

Table 4 shows the values of recognition parameters calculated by the formulas Q —(3), (19), Z_{eff} —(13), and (14) for materials from Table 1, supplemented with data for polyvinyl chloride and polyvinylidene fluoride.

From the data analysis in Table 4, we can conclude that water and borax can act as the material associated with the class of explosives. The proximity of sugar to the class of explosives should also be noted in terms of the analyzed recognition parameters. The differences between the maximum and minimum Z_{eff} values for the analyzed explosives are practically independent of the pairs of gamma radiation energies E_L and E_H .

Table 4. Values of recognition parameters for materials from Table 1.

Material	$E_L = 1 \text{ MeV},$ $E_H = 4 \text{ MeV}$		$E_L = 2 \text{ MeV},$ $E_H = 5 \text{ MeV}$		$E_L = 2 \text{ MeV},$ $E_H = 6 \text{ MeV}$		$E_L = 3 \text{ MeV},$ $E_H = 6 \text{ MeV}$		$E_L = 4 \text{ MeV},$ $E_H = 7 \text{ MeV}$	
	Q	Z_{eff}	Q	Z_{eff}	Q	Z_{eff}	Q	Z_{eff}	Q	Z_{eff}
Polyethylene	0.474	4.397	0.601	4.71	0.545	4.607	0.683	4.57	0.747	4.394
Carbon (graphite)	0.479	5.741	0.61	5.99	0.556	5.9	0.693	5.86	0.759	5.726
Sugar	0.48	6.099	0.612	6.34	0.559	6.245	0.696	6.208	0.762	6.091
Water	0.481	6.333	0.613	6.57	0.561	6.47	0.698	6.435	0.764	6.329
Trinitrotoluene	0.482	6.563	0.615	6.78	0.562	6.692	0.7	6.656	0.766	6.553
RDX	0.482	6.593	0.615	6.8	0.563	6.72	0.7	6.684	0.766	6.583
C-4	0.483	6.728	0.616	6.93	0.564	6.849	0.701	6.814	0.767	6.718
Pentrite	0.483	6.892	0.617	7.1	0.565	7.009	0.702	6.973	0.769	6.882
Borax	0.484	7.096	0.618	7.31	0.567	7.215	0.704	7.175	0.771	7.096
Polyvinylchloride	0.499	11.28	0.645	11.38	0.6	11.32	0.737	11.29	0.806	11.27
Polyvinylidene fluoride	0.484	7.167	0.619	7.4	0.567	7.307	0.705	7.263	0.771	7.175
Fluoropolymer	0.487	8.084	0.625	8.3	0.575	8.204	0.712	8.158	0.779	8.096
Albite	0.497	10.63	0.641	10.71	0.595	10.64	0.732	10.62	0.8	10.6
Quartz	0.497	10.75	0.641	10.81	0.596	10.75	0.732	10.74	0.801	10.7
Aluminum	0.505	12.99	0.656	13.05	0.614	12.99	0.75	12.95	0.82	13.01
Dolomite	0.497	10.79	0.642	10.87	0.596	10.81	0.733	10.78	0.801	10.75
Calcite	0.504	12.52	0.653	12.56	0.61	12.52	0.746	12.48	0.815	12.47
Fluorite	0.512	14.81	0.667	14.83	0.629	14.79	0.764	14.76	0.833	14.77
Rutile	0.517	16.12	0.676	16.11	0.639	16.04	0.773	16.01	0.843	16.04
Pyrite	0.533	20.57	0.703	20.45	0.674	20.45	0.806	20.46	0.876	20.52
Iron	0.552	26.21	0.738	26	0.717	26.02	0.844	26.07	0.913	26.13
Tin	0.614	49.74	0.863	50	0.871	50.08	0.972	50.21	1.026	50.39
Tantalum	0.612	48.41	0.925	73.06	0.949	72.17	1.032	71.83	1.074	70.76

4.2. Material Recognition Using the High-Energy Dual-Energy Method

Works [5,12,14,15,29] note the existence of ranges of variations in the thicknesses of TO fragments in the MFP for lower E_L bremsstrahlung energy or their mass thicknesses, which correct material recognition is problematic. This problem is manifested in the proximity of the average values of the PR Q for two or more classes in a certain subrange of the area of consumer interest in relation to the TO thicknesses in MFP (mass thicknesses). The use of preliminary filtering of bremsstrahlung significantly increases the thicknesses range of the correct recognition of materials [5].

Detection of large explosive traps [44,45] and their correct recognition is one of the main purposes of inspection control in relation to anti-terrorist activities, security of transport, transport facilities, and highways.

The consumer is interested in the thickness range of fragments from explosives H , for which the fragment's material, according to one or another recognition parameter, correctly belongs to the class of heavy organic materials.

As an example, consider the thickness range of trinitrotoluene (TNT) H_{TNT} fragments from 100 mm to 300 mm. Since the TO density ρ_{TNT} is equal to 1.65 g/cm^3 , we study the range of changes in the mass thicknesses of TO ρH from 16.5 g/cm^2 to 49.5 g/cm^2 .

As an example, let us choose a HEIS with the following structural elements: RSE made of cadmium tungstate (CdWO_4) with a density of $\rho_d = 7.91 \text{ g/cm}^3$ and a thickness of $h_d = 35 \text{ mm}$; pre-filter made of iron (Fe) $h_f = 30 \text{ mm}$ thick; bremsstrahlung source with maximum bremsstrahlung energies $E_L = 5 \text{ MeV}$ and $E_H = 9 \text{ MeV}$; digital detector with ADC bit depth $k_{ADC} = 24$ and matching ratio of the ranges of change in analog and digital signals $C_{ADC} = 0.8$.

4.2.1. An Example of Calculating the Material Recognition Parameter by the Level Lines Method

Table 5 shows the results of calculations of the material recognition parameter Q for the DEM implementation by the level lines method for the above-described HEIS.

Table 5. Recognition parameters Q for fragments of the mass thickness ρH , explosives are highlighted in red.

Material	$\rho H, \text{g/cm}^2$				
	16.5	24.75	33	41.25	49.5
Polyethylene	0.7772	0.7753	0.7737	0.7723	0.7712
Graphite	0.7818	0.7803	0.7789	0.7783	0.7772
Sugar	0.7829	0.7813	0.7802	0.779	0.7785
Water	0.7834	0.782	0.7811	0.7798	0.7794
Trinitrotoluene	0.7844	0.7829	0.782	0.781	0.7805
RDX	0.7846	0.7831	0.7821	0.7812	0.7803
C-4	0.7847	0.7835	0.7827	0.7819	0.7812
Pentrite	0.7854	0.784	0.7832	0.7825	0.7818
Borax	0.7859	0.7848	0.7839	0.783	0.7824
Polyvinylchloride	0.7986	0.7985	0.7982	0.7985	0.7988
Polyvinylidene fluoride	0.7865	0.7852	0.7843	0.7834	0.7828
Fluoropolymer	0.789	0.7884	0.7877	0.787	0.7868
Albite	0.7967	0.7964	0.796	0.796	0.7961
Quartz	0.797	0.7966	0.7963	0.7966	0.7963
Aluminum	0.8039	0.8041	0.8039	0.8046	0.8048
Dolomite	0.7973	0.7968	0.7965	0.7965	0.7968
Calcite	0.8021	0.8021	0.8024	0.8025	0.8032
Fluorite	0.809	0.8095	0.8099	0.8108	0.8112
Rutile	0.8126	0.8133	0.8143	0.8152	0.8158
Pyrite	0.8251	0.8266	0.8281	0.8296	0.831
Iron	0.8395	0.842	0.8445	0.8466	0.8485
Tin	0.881	0.8882	0.8942	0.8989	0.903
Tantalum	0.8877	0.9015	0.9114	0.9193	0.9257

For light and heavy organic materials, as well as light inorganic materials, there is a fairly significant decrease in the value of the PR Q with an increasing mass thickness of TO fragments. The Q values for all analyzed explosives are close to each other. From the data obtained, it can be concluded that it is possible to distinguish the class of heavy organic materials (typical representatives—water, polyvinylidene fluoride, or borax) from light organic materials (polyethylene) and from light inorganic materials (fluoropolymer) by parameter Q .

4.2.2. An Example of Calculating the Effective Atomic Number

Table 6 shows the results of calculating the effective atomic number for the conditions of the example noted above. The data given in Table 5 differ significantly from the data in Table 1 due to the high-energy DEM implementation. Nevertheless, an analysis of the table allows us to confirm that it is possible to increase the number of material recognition classes by introducing a class of heavy organic materials with a range of Z_{eff} from 6.47 (water) to 7.27 (borax).

Table 6. Calculation of the effective atomic number for materials from Table 1, explosives are highlighted in red.

Material	$\rho H, \text{g/cm}^2$				
	16.5	24.75	33	41.25	49.5
Polyethylene	4.715	4.89	4.75	4.68	4.715
Graphite	5.87	5.94	6.01	6.01	5.94
Sugar	6.395	6.29	6.325	6.22	6.36
Water	6.535	6.605	6.5	6.5	6.57
Trinitrotoluene	6.745	6.71	6.78	6.815	6.78
RDX	6.815	6.78	6.745	6.815	6.78
C-4	6.92	6.955	6.99	6.99	6.99
Pentrite	7.27	7.235	7.235	7.06	7.06
Borax	7.41	7.34	7.305	7.27	7.235
Polyvinylchloride	11.4	11.23	11.26	11.3	11.33
Polyvinylidene fluoride	7.375	7.41	7.34	7.375	7.34
Fluoropolymer	8.25	8.15	8.18	8.285	8.25
Albite	10.67	10.67	10.67	10.77	10.63
Quartz	10.95	10.74	10.74	10.84	10.7
Aluminum	12.94	12.94	12.98	12.98	12.98
Dolomite	10.91	10.88	10.84	10.81	10.81
Calcite	12.73	12.59	12.52	12.45	12.42
Fluorite	14.87	14.8	14.73	14.66	14.87
Rutile	15.99	15.85	16.02	15.92	16.02
Pyrite	20.4	20.4	20.33	20.47	20.36
Iron	26.17	26.03	26.	25.93	26.07
Tin	49.83	50.01	50.11	49.9	49.97
Tantalum	72.93	68.70	72.65	72.97	72.76









5. Simulation

The mathematical model described in the first section is implemented in the MathCad system for mathematical calculations. A library [40] of gamma-ray attenuation data is used to create the primary DEM images.

Recall that the purpose of the simulation was to evaluate the possibility of detecting and correcting the detection of solid materials that are close in effective atomic number to explosives.

Table 7 shows an extended classification of materials in relation to the considered problem, indicating the typical representative of the class, the corresponding range of changes in the effective atomic number, the materials of the class, and the selected color in the additive color model RGB. The proposed palette is generally close to the palette of [3]. The proposed palette is generally close to that of [3]. The red color corresponds to the class of heavy organic materials, as this color traditionally indicates increased danger.

Table 7. Extended classification of materials by the dual-energy method.

Z_{eff}	Class of Materials	Material	Color	RGB
2.1–6.1	Light organic materials	Polyethylene		(0, 255, 255)
6.1–7.8	Heavy organic materials	Explosives		(255, 0, 0)
7.8–10.5	Heavy plastics, light metal oxides, and salts	Fluoropolymer		(255, 0, 255)
10.5–15	Light metals	Aluminum		(0, 255, 0)
15–22	Heavy inorganic materials	Calcium oxide		(255, 255, 0)
22–30	Heavy metals	Steel		(0, 0, 255)
30–57	Metals with a high atomic number	Tin		(255, 0, 255)
57+	Non-transparent materials	Tantalum		(128, 128, 128)

According to the data given above, a virtual test object consisting of fragments with mass thickness from ρH from $(\rho H)_{min} = 15 \text{ g/cm}^2$ (100 mm TNT) to $(\rho H)_{max} = 99 \text{ g/cm}^2$ (600 mm TNT) was formed in 7 g/cm^2 increments. We used the set of fragment materials from Table 7, supplemented with explosives from Table 1, water, and borax. The fragments in the test object are grouped into a matrix, each row of which is associated with one material.

The following sequence of materials is considered: polyethylene; water; trinitrotoluene; RDX; C-4; pentrite; borax; fluoropolymer, aluminum; calcium oxide; iron; tin; tantalum. The choice of this set of materials is due to their relative availability. The simulation was performed on a Tomsk Polytechnic University digital simulator (TPU) [46] for a pair of maximum energies of the bremsstrahlung radiation $E_L = 5 \text{ MeV}$ and $E_H = 9 \text{ MeV}$ with an increased ADC bit depth $k_{ADC} = 24$. The simulation of the recognition of materials of TO fragments was performed [6,29,47], taking into account the partial alignment of the ranges of variation in analog signals for lower and higher maximum energies of the bremsstrahlung radiation, as well as the partial agreement of the ranges of variation in analog and digital signals. The value of the parameter N_{1L} , which determines the noise level of the recognition parameters, ranged from 5×10^3 to 2×10^6 . The approach based on analog integration of several radiation pulses was used to align the ranges of variation in analog signals for $E_L = 5 \text{ MeV}$ and $E_H = 9 \text{ MeV}$ and match the ranges of variation in analog and digital signals.

Figure 3 shows images of the EAN distribution for the TO described above, supplemented with fragments from the explosive materials indicated in Table 1. The visualization of EAN was made considering the mass thicknesses of the fragments of the test object. The smaller the mass thickness of the fragment, the brighter its image.

From the analysis of the obtained data, we can conclude that it is possible to isolate fragments from the class of heavy organic materials (explosives and their simulants) in the range of 100 mm thickness from TNT. A sufficient level of radiation transparency of the fragment of the explosive of interest and a sufficient level of the parameter N_0 determine the upper limit.

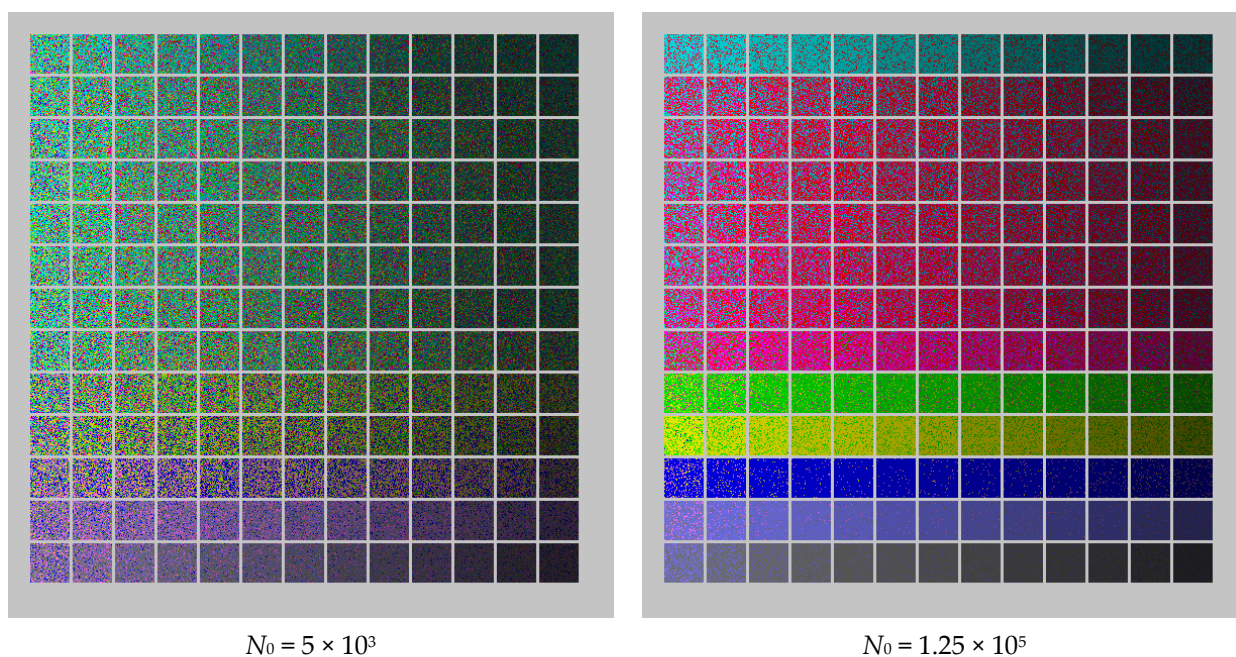


Figure 3. Cont.

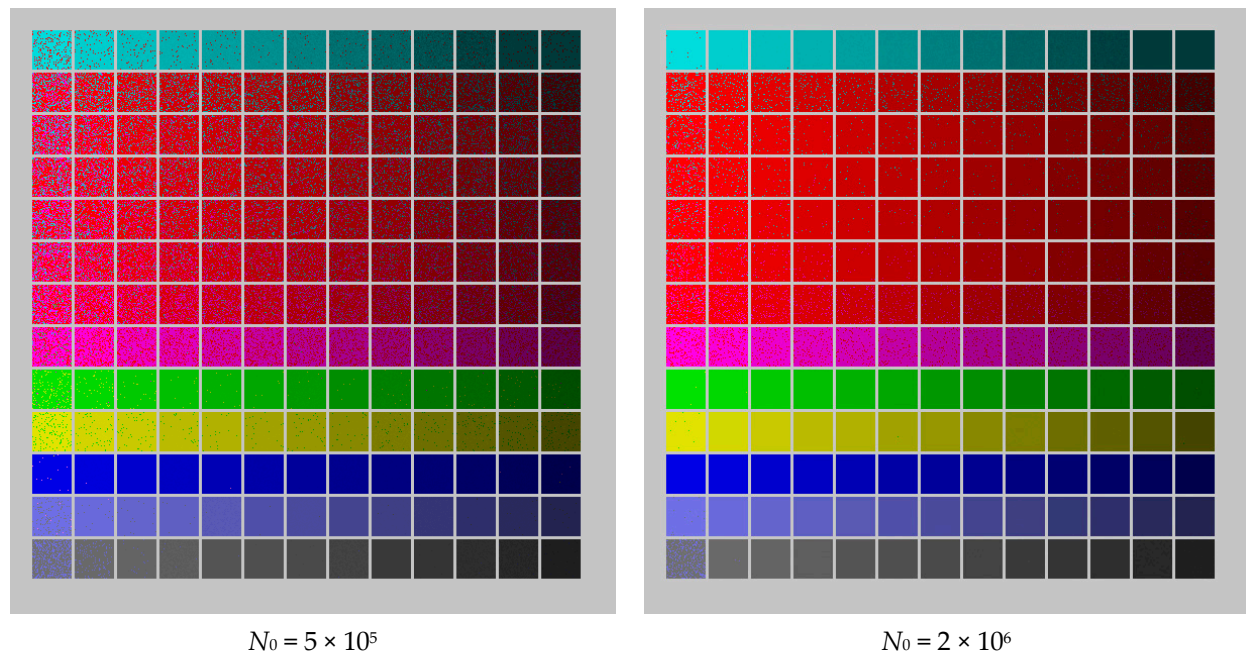


Figure 3. Images of the EAN distribution, taking into account the mass thickness of the fragments.

6. Discussion

6.1. General Recommendations

In previous papers, the authors [3,8,10] noted that the probability of correct recognition increases with the rational choice of the following parameters: the pair of maximum X-ray radiation energies E_L , E_H ; the resolution of the ADC k_{ADC} ; and the number of photons falling on the frontal surfaces of the RSE detectors N_{L0} and N_{H0} . Of course, it is necessary to comply with all the requirements for all kinds of calibrations characteristic of a HEIS with dual or multi-energy material recognition function [1,5,11].

It should be noted that the quality of material recognition significantly depends on the accuracy of the solution of the system (15). Non-monotonicity of the dependences y_L and y_H on the atomic number Z leads to a significant dependence of the accuracy and uniqueness of the solution (15) on the initial approximation, which limits the use of MathCad built-in tools for solving systems of equations. In [5], an approach based on the system's transformation (15), which practically eliminates the ambiguity of the EAN estimation and significantly increases the accuracy of this estimate, was applied. Let us elaborate on this approach.

6.2. Increasing the Accuracy of Effective Atomic Number Estimation

It is known [2,5,8,14] that in certain ranges of variation Z_{eff} , the recognition parameter Q is a smooth function of Z_{eff} . This is due to the presence of such a range for the monoenergetic DEM realization, see Figure 1.

The system of nonlinear Equation (15) can be transformed into the following system

$$\begin{aligned} F_Q(y, Z_{eff}) &= Q \\ F_{\rho H}((\rho H)_{eff}, Z_{eff}) &= y_L \end{aligned} \quad (20)$$

where $F_Q(y, Z_{eff})$, $F_{\rho H}((\rho H)_{eff}, Z_{eff})$ are special DEM calibration functions formed from the initial calibration data for the maximum bremsstrahlung energies E_L and E_H . Here, the subscript Q is associated with the transformation of functions from system (15) to (9), and the subscript ρH indicates the greater significance of the corresponding function on the ρH .

It follows from the first equation of the system (20) that its solution with respect to Z_{eff} exists only in the monotonicity section of the function $F_Q(y, Z_{eff})$. Otherwise, the decision (20) relative to Z_{eff} will be ambiguous.

We describe the process of special calibration.

Let there be discrete sets of mass thicknesses $\rho\mathbf{H} = \{(\rho H)_i, i = 1 \dots i_0\}$ and effective atomic numbers $\mathbf{Z} = \{Z_j, j = 1 \dots j_0\}$. These sets correspond to the matrix $\rho\mathbf{H}\mathbf{Z} = \{((\rho H)_i, Z_j), i = 1 \dots i_0, j = 1 \dots j_0\}$. As a result of experimental measurements and subsequent calibrations, the matrices \mathbf{y}_{CL} and \mathbf{y}_{CH} are formed.

A special calibration algorithm.

1. In accordance with Formula (9), the calibration matrix of the recognition parameter \mathbf{Q}_C is constructed.
2. In the monotonically increasing section along Z , there is a two-dimensional continuous function $F_Q(y, Z_{eff})$ interpolating (approximating) the discrete dependence described by the set of matrices \mathbf{Q}_C and \mathbf{y}_{CL} . The first argument in the function is the thickness of the attenuating object in mean path lengths for X-rays with the maximum energy E_L , and the second argument is the EAN value. Polynomials can be used as an interpolating function [48].
3. For the above section of a monotonous increase in Z , there is a two-dimensional function $F_{\rho H}((\rho H)_{eff}, Z_{eff})$.

The specifics of the solution to system (20) is that the first equation of the system turns into an equation with one unknown and has a pronounced geometric interpretation. Nevertheless, taking into account the described conditions and restrictions, the solution regarding Z_{eff} is unambiguous, and the accuracy is determined primarily by measurement noise, the quality of the primary calibrations, the degree of collimation of radiation, and the number of breakdown points by the EAN of materials and the mass thickness of TO fragments for DEM calibration.

The second equation of the system (2), after the substitution of the Z_{eff} value obtained from the first equation, also becomes one-dimensional and is easily solved relatively $(\rho H)_{eff}$.

The models under consideration make it possible to obtain a fairly accurate estimate of the mass thickness of the TO fragments, and the integration over the area of the fragment makes it possible to estimate its mass. Simultaneous recognition of explosives with the estimation of their mass and combined with other methods [49] will significantly increase the level of transport security and reduce the associated risks.

6.3. Comparison with Related Works

The studies presented in the paper are a natural continuation and development of the series of articles [5,8,10,29,35,43] devoted to mathematical and simulation modeling of various DEM implementations. In this work, the mathematical and simulation models of DEM implementations were refined both in terms of level line parameters and in terms of effective atomic numbers. The refinement was reduced to introducing a highly accurate and highly productive algorithm for estimating the effective atomic number of a material using the level line method into the mathematical model, to developing an approach to determining the ultimate capabilities of high-energy DEMs, which made it possible to carry out a cycle of the necessary computational experiments and, based on the analysis of their results, draw a conclusion about the fundamental possibility of reliably distinguishing the class of heavy organic materials from light organic materials and from light inorganic materials using the recognition parameters Q and Z_{eff} . The available [5,8,10,29,35,43] results of experimental estimates of the recognition parameters (Q and Z_{eff}) are less accurate compared to those noted above. Over the last decade, the main direction of HEIS develop-

ment with the dual-energy material recognition function has been to increase inspection performance, which has held back research in other areas, such as more accurate Z_{eff} estimation, expansion of the ranges of mass thicknesses of the OC, an increase in the number of classes of reliably recognized materials, etc. It should be noted that in recent years, the interest of scientists and practitioners in mathematical modeling of the analyzed systems has grown significantly, which is certainly associated with the urgent need to improve the accuracy of estimating the effective atomic numbers of OC materials and increasing the number of material recognition classes when inspecting cargo using the high-energy X-ray dual-energy method. Among the latest works devoted to the above-mentioned topics, one can note [50]; however, the accuracy of Z_{eff} estimation leaves much to be desired, the error is up to several units of EAN, which is significantly worse than in the presented work. The reason for the high error in the EAN estimation, in our opinion, is the use of the Alvarez–Makovsky method in the mathematical model, which is characterized by noticeable systematic biases in the Z_{eff} estimates. The theoretical model for estimating Z_{eff} from [4] also uses the Alvarez–Makovsky method; visually, fragments from materials similar to those considered in this work are well-recognized, but there are no data on Z_{eff} . The approach used in [27] is close to the model described above. The experimental data on the Q parameter are close to those given above, but the experiments and calculations were carried out in [27] only for four classes of recognizable materials.

7. Conclusions

Issues related to increasing the number of material recognition classes by the dual high-energy method by introducing a class of heavy organic materials, which includes basic explosives, are considered. A mathematical model of material recognition by the dual-energy method based on the parameters of level lines and effective atomic numbers was proposed. Estimates of the parameters of the level lines and effective atomic numbers of explosives and their physical counterparts for monoenergetic and classical high-energy implementations of the dual-energy method were made. The use of a simulation model to demonstrate the ability to detect and correctly identify explosives and their physical counterparts using the dual high-energy method is illustrated. An algorithmic methodological approach is proposed to improve the accuracy of the effective number estimation. It was proved theoretically and by simulation that it is possible to distinguish materials from the following classes of materials: light organics (typical representative—polyethylene); heavy organics (explosives), light minerals and heavy plastics (fluoropolymers); light metals (aluminum, $Z = 13$), heavy minerals (calcium oxide, $Z = 19$); metals (iron, $Z = 26$); heavy metals (tin, $Z = 50$); and radiation insensitive metals ($Z > 57$).

The dual-energy method improves the detection of explosives in transport and transported cargo by introducing a special class of recognizable materials, called the class of heavy organic materials, strictly taking into account all the physical laws of interaction of high-energy bremsstrahlung with matter, rational selection of technical parameters of the corresponding inspection control systems, ensuring high-quality calibrations at all stages of the formation and processing of DEM images.

In the future, we plan to implement a number of research topics related to the substantiation of the possibility of increasing the efficiency of high-energy, dual- and multi-energy methods, as well as spectral methods for the correct (separate) recognition of organic and inorganic materials based on the assessment of their effective atomic numbers.

Author Contributions: Methodology, S.O. and E.U.; Software, S.C.; Formal analysis, S.C.; Writing—original draft, S.O., S.C. and E.U.; Writing—review and editing, E.U.; Project administration, S.O. All authors have read and agreed to the published version of the manuscript.

Funding: This study has been conducted under the financial support by the Ministry of Science and Higher Education of the Russian Federation within the state task “Research” (basic fundamental), project # FSWW-2023-0004.

Institutional Review Board Statement: Not applicable.

Informed Consent Statement: Not applicable.

Data Availability Statement: Dataset available on request from the authors.

Conflicts of Interest: Authors Sergey Osipov and Eugeny Usachev were employed by the company Diagnostika-M LLC. The remaining authors declare that the research was conducted in the absence of any commercial or financial relationships that could be construed as a potential conflict of interest.

References

1. Ghaebi, M.; Tajik, M.; Azimirad, R. Studying the effect of the scanned objects’ location on material discrimination in a dual-energy cargo inspection system. *Nucl. Instrum. Methods Phys. Res. B* **2022**, *510*, 9–48. [CrossRef]
2. Kayalvizhi, R.; Kumar, A.; Malarvizhi, S.; Topkar, A.; Vijayakumar, P. Raw data processing techniques for material classification of objects in dual energy X-ray baggage inspection systems. *Radiat. Phys. Chem.* **2022**, *193*, 109512. [CrossRef]
3. Benedykciuk, E.; Denkowski, M.; Dmitruk, K. Material classification in X-ray images based on multi-scale CNN. *Signal Image Video Process.* **2021**, *15*, 1285–1293. [CrossRef]
4. Fang, W.; Li, L. Attenuation image referenced (AIR) effective atom number image calculation for MeV dual-energy container CT using image-domain deep learning framework. *Results Phys.* **2022**, *35*, 105406. [CrossRef]
5. Osipov, S.P.; Usachev, E.Y.; Chakhlov, S.V.; Shchetinkin, S.A.; Song, S.; Zhang, G.; Batranin, A.V.; Osipov, O.S. Limit capabilities of identifying materials by high dual- and multi-energy methods. *Russ. J. Nondestruct. Test.* **2019**, *55*, 687–699. [CrossRef]
6. Saverskiy, A.Y.; Dinca, D.C.; Rommel, J.M. Cargo and container X-ray inspection with intra-pulse multi-energy method for material discrimination. *Phys. Procedia* **2015**, *66*, 232–241. [CrossRef]
7. Arodzero, A.; Boucher, S.; Kutsaev, S.V.; Lanza, R.C.; Palermo, V.; O’Shea, F.; Ziskin, V. MEBCIS: Multi-energy betatron-based cargo inspection system. In Proceedings of the 2016 IEEE Nuclear Science Symposium, Medical Imaging Conference and Room-Temperature Semiconductor Detector Workshop (NSS/MIC/RTSD), Strasbourg, France, 29 October–6 November 2016; IEEE: Strasbourg, France, 2016; pp. 1–5. [CrossRef]
8. Osipov, S.P.; Usachev, E.J.; Chakhlov, S.V.; Schetinkin, S.A.; Osipov, O.S. Inspection of bulk cargoes and liquids by the dual energy method. *Radiat. Phys. Chem.* **2020**, *177*, 109133. [CrossRef]
9. Mery, D.; Pieringer, C. *X-Ray Testing. Computer Vision for X-Ray Testing*; Springer: Cham, Switzerland, 2021; pp. 1–41. [CrossRef]
10. Osipov, S.; Chakhlov, S.; Osipov, O.; Shtein, A.; Van, J. Adequacy criteria of models of the cargo inspection system with material discrimination option. *J. Phys. Conf. Ser.* **2016**, *671*, 012010. [CrossRef]
11. Moshkbar-Bakhshayesh, K.; Afarideh, H.; Mohtashami, S.; Azimirad, R. Inspection of Cargo Using Dual-Energy X-Ray Radiography: A Review. *Radiat. Phys. Chem.* **2023**, *212*, 111180. [CrossRef]
12. Lee, T.B.; Kang, H.S. Material Estimation Method Using Dual-Energy X-Ray Image for Cargo Inspection System. *J. Korea Ind. Inf. Syst. Res.* **2018**, *1*, 1–12. [CrossRef]
13. Turturica, G.V.; Iancu, V.; Ur, C.A. A neural-network based approach to cargo inspections using photon spectroscopy. *Nucl. Instrum. Methods Phys. Res. A Accel. Spectrom. Detect. Assoc. Equip.* **2021**, *1010*, 165553. [CrossRef]
14. Ogorodnikov, S.; Petrunin, V. Processing of interlaced images in 4–10 MeV dual energy customs system for material recognition. *Phys. Rev. Accel. Beams* **2002**, *5*, 104701. [CrossRef]
15. Chen, Z.Q.; Zhao, T.; Li, L. A curve-based material recognition method in MeV dual-energy X-ray imaging system. *JNST* **2016**, *27*, 25. [CrossRef]
16. Rapiscan Systems. Cargo & Vehicle Inspection. Available online: <https://www.rapiscansystems.com/en/products/category/cargo-and-vehicle-inspection> (accessed on 25 November 2024).
17. NUCTECH. Europe. Cargo Inspection & Vehicle Scanners. Available online: <https://nuctecheuropa.com/products/cargo-container> (accessed on 27 November 2024).
18. LINEV Systems US, Inc. DTP 7500/200UV. Available online: <https://linevsystems.us/product/dtp-7500-200uv/> (accessed on 26 November 2024).
19. Smiths Detections. Cargo & Vehicle Inspection. Available online: <https://www.smithsdetection.com/product-finder/cargo-vehicle-inspection> (accessed on 25 November 2024).
20. Diagnostika-M LLC. Digital Systems and Installations. Available online: <https://en.tsnk.ru/equip/equip/digital-systems-and-installations/> (accessed on 27 November 2024).
21. Scantronic Systems. Available online: <https://scantronicsystems.com/en/catalog/> (accessed on 27 November 2024).

22. Duvillier, J.; Dierick, M.; Dhaene, J.; Van Loo, D.; Masschaele, B.; Geurts, R.; Van Hoorebeke, L.; Boone, M.N. Inline multi-material identification via dual energy radiographic measurements. *NDT&E Int.* **2018**, *94*, 120–125. [CrossRef]
23. Yalçın, O.; Reyhancan, İ.A. Detection of explosive materials in dual-energy X-Ray security systems. *Nucl. Instrum. Methods Phys. Res. A Accel. Spectrom. Detect. Assoc. Equip.* **2022**, *1040*, 167265. [CrossRef]
24. Çıgla, C.; Küçükates, B.; Yalçın, O.; Ak, D.S.; Işıkoğlu, Ş.T. Robust material classification on dual-energy x-ray imaging devices. Anomaly Detection and Imaging with X-Rays (ADIX) VII. *SPIE* **2022**, *12104*, 18–34. [CrossRef]
25. Hubbell, J.H. *Photon Cross Sections, Attenuation Coefficients, and Energy Absorption Coefficients from 10 keV to 100 GeV*; U.S. Department of Commerce, The National Standard Reference Data System: Washington, DC, USA, 1969.
26. Hubbell, J.H. Electron-positron pair production by photons: A historical overview. *Radiat. Phys. Chem.* **2006**, *75*, 614–623. [CrossRef]
27. Rogers, T.W.; Jaccard, N.; Morton, E.J.; Griffin, L.D. Automated X-ray image analysis for cargo security: Critical review and future promise. *J. X-Ray Sci. Technol.* **2017**, *25*, 33–56. [CrossRef]
28. Zhvyrbliia, V.Y.; Osipov, S.P.; Sednev, D.A. Increasing penetrating power of digital radiography systems based on analysis of low-intensity signals. *Russ. J. Nondestruct. Test.* **2022**, *58*, 583–597. [CrossRef]
29. Osipov, S.P.; Chakhlov, S.V.; Osipov, O.S.; Li, S.; Sun, X.; Zheng, J.; Hu, X.; Zhang, G. Physical and technical restrictions of materials recognition by the dual high energy X-ray imaging. *Int. J. Appl. Eng. Res.* **2017**, *12*, 13127–13136.
30. Barnes, S.; Georgadze, A.; Giammanco, A.; Kiisk, M.; Kudryavtsev, V.A.; Lagrange, M.; Pinto, O.L. Cosmic-Ray Tomography for Border Security. *Instruments* **2023**, *7*, 13. [CrossRef]
31. Kahani, M. Dose Evaluation of a Car Occupant in Dual Energy X-Ray Automobile Inspection System. *Medicon Med. Sci.* **2022**, *2*, 33–41. [CrossRef]
32. Park, J.Y.; Mun, J.; Lee, J.H.; Yeon, Y.-H.; Chae, M.; Lee, M.; Lee, N.-H. Development of a Dual-Modality Gamma-ray/Fast Neutron Imaging System for Air Cargo Inspection. *Appl. Sci.* **2022**, *12*, 9775. [CrossRef]
33. Alves, H.; Lima, I.; de Assis, J.T.; Neves, A.A.; Lopes, R.T. Mineralogy evaluation and segmentation using dual energy microtomography. *X-Ray Spectrom.* **2015**, *44*, 99–104. [CrossRef]
34. Bonnin, A.; Duvauchelle, P.; Kaftandjian, V.; Ponard, P. Concept of effective atomic number and effective mass density in dual-energy X-ray computed tomography. *Nucl. Instrum. Methods Phys. Res. B* **2014**, *22*, 223–231. [CrossRef]
35. Osipov, S.; Chakhlov, S.; Udod, V.; Usachev, E.; Schetinkin, S.; Kamysheva, E. Estimation of the effective mass thickness and effective atomic number of the test object material by the dual energy method. *Radiat. Phys. Chem.* **2020**, *168*, 108543. [CrossRef]
36. Bauer, C.; Wagner, R.; Leisner, J. Foreign body detection in frozen food by dual energy X-ray transmission. *Sens. Transducers* **2021**, *253*, 23–30.
37. Heckert, M.; Enghardt, S.; Bauch, J. Novel multi-energy X-ray imaging methods: Experimental results of new image processing techniques to improve material separation in computed tomography and direct radiography. *PLoS ONE* **2020**, *15*, e0232403. [CrossRef]
38. Haase, V.; Noo, F.; Stierstorfer, K.; Maier, A.; McNitt-Gray, M. Reproducibility in dual energy CT: The impact of a projection domain material decomposition method. 7th International Conference on Image Formation in X-Ray Computed Tomography. *SPIE* **2022**, *12304*, 101–106. [CrossRef]
39. Ilkukhin, N.J.; Moskvina, S.V. Simulators of explosives to test the performance of technical means of security based on the methods of X-ray and neutron radiation analysis. *Probl. Def. Technol. Ser. 16 Tech. Means Countering Terror.* **2016**, *3–4*, 76–81. (In Russian)
40. Berger, M.J.; Hubbell, J.H.; Seltzer, S.M.; Chang, J.; Coursey, J.S.; Sukumar, R.; Zucker, D.S.; Olsen, K. *XCOM: Photon Cross Sections Database, NIST Standard Reference Database 8 (XGAM); (Version 1.5); The U.S. Secretary of Commerce: Washington, DC, USA, 2010.* [CrossRef]
41. Cao, W.; Sun, T.; Kerckhofs, G.; Fardell, G.; Price, B.; Dewulf, W. A simulation-based study on the influence of the X-ray spectrum on the performance of multi-material beam hardening correction algorithms. *Meas. Sci. Technol.* **2018**, *29*, 095002. [CrossRef]
42. Martini, M.; Francus, P.; Trotta, D.S.L.; Despres, P. Identification of Common Minerals Using Stoichiometric Calibration Method for Dual-Energy CT. *Geochem. Geophys. Geosyst.* **2021**, *22*, e2021GC009885. [CrossRef]
43. Osipov, S.P.; Usachev, E.Y.; Chakhlov, S.V.; Shchetinkin, S.A.; Osipov, O.S. Specific features of material recognition by the multi-energy X-Ray method. *Russ. J. Nondestruct. Test.* **2019**, *55*, 308–321. [CrossRef]
44. Zentai, G. X-ray imaging for homeland security. *IEEE Int. Workshop Imaging Syst. Tech.* **2008**, *3*, 13. [CrossRef]
45. Lehnert, A.L.; Kearfott, K.J. The Detection of Explosive Materials: Review of Considerations and Methods. *Nucl. Technol.* **2010**, *172*, 325–334. [CrossRef]
46. Scientific Educational Cargo Vehicle Inspection System. Available online: <https://rkd.tpu.ru/en/developments/inspection/> (accessed on 27 November 2024).
47. Kutsaev, S.; Agustsson, R.; Arodzero, A.; Berry, R.; Bezhanov, A.; Boucher, S.; Chimalpopoca, O.; Diego, A.; Faillace, L.; Gavryushkin, D.; et al. Compact X-Band electron linac for radiotherapy and security applications. *Radiat. Phys. Chem.* **2021**, *185*, 109494. [CrossRef]

48. Chang, C.H.; Ni, Y.C.; Tseng, S.P. Calculation of effective atomic numbers using a rational polynomial approximation method with a dual-energy X-ray imaging system. *J. X-Ray Sci. Technol.* **2021**, *29*, 317–330. [[CrossRef](#)]
49. Nabiev, S.S.; Palkina, L.A. Modern technologies for detection and identification of explosive agents and devices. *Russ. J. Phys. Chem. B* **2017**, *11*, 729–776. [[CrossRef](#)]
50. Lalor, P.; Danagouliau, A. Atomic number estimation of dual energy cargo radiographs using a semiempirical transparency model. *Nucl. Instrum. Methods Phys. Res. A Accel. Spectrom. Detect. Assoc. Equip.* **2024**, *1064*, 169343. [[CrossRef](#)]

Disclaimer/Publisher’s Note: The statements, opinions and data contained in all publications are solely those of the individual author(s) and contributor(s) and not of MDPI and/or the editor(s). MDPI and/or the editor(s) disclaim responsibility for any injury to people or property resulting from any ideas, methods, instructions or products referred to in the content.